Drying Front and Vaporization Plane Dynamics during Evaporation from Homogeneous Soil Profiles

Jumana Hussary[1*], *Adel* Alowaisy[1], *Noriyuki* Yasufuku[1], *Ryohei* Ishikura[1], and *Monther* Abdelhadi[2]

[1]Department of Civil Engineering, Faculty of Engineering, Kyushu University, Fukuoka, Japan
[2]Department of Civil Engineering, Faculty of Engineering, American University of Madaba, Madaba, Jordan

Abstract. Global warming has caused many lands to degrade, making them vulnerable to desertification. Therefore, finding innovative solutions is essential to prevent such phenomena from exacerbating. However, this requires a comprehensive understanding of the unsaturated layer formed due to the high-water loss from soil profiles by evaporation. In the present study, a new technique to trace the unsaturated layer from drying soil profiles was developed, and its accuracy and reliability were confirmed. Consequently, the spatial and temporal development of the drying front, vaporization plane, and film region were investigated for two soil profiles of different pore structures. It was found that soil profiles with broader pore distribution lose water from deeper drying fronts during Stage 1, while diffusion during Stage 2 occurs from shallower depths. Moreover, the film region's thickness increased at early drying stages, followed by a slight drop associated with the onset of Stage 2. During Stage 2, the thickness slightly fluctuated until reaching the same thickness at the end of Stage 1, where a second significant drop in the thickness was observed.

1 Introduction

Global warming ramifications have led an approximation of 45% of the world's lands to degrade and lose their soil's productive capacity. Optimizing innovative solutions to prevent such environmental disasters requires a thorough understanding and accurate prediction of the water fluxes, especially evaporation that dominates in drylands [1, 2]. However, this has been a great challenge due to the complexity associated with the governing pore-scale mechanisms and influencing factors on evaporation.

From a macroscale perspective, the evaporation process involves three stages. The constant rate stage (Stage 1) is characterized by the highest and relatively constant actual evaporation rate, followed by a lower receding rate through the falling rate stage (Stage 2), and finally, the residual stage (Stage 3), which is identified once the rate converges to a constant and low value. From a microscale perspective, evaporation is conceptualized based on the water transport mechanism governed by the dynamics of the unsaturated layer. During Stage 1, the evaporation is sustained by capillary flow from the drying front, the region between the saturated and unsaturated zones, to the surface. At a specific drying front depth, the hydraulic connection with the surface is disrupted [3]. Consequently, a new vaporization plane is formed below the soil surface announcing Stage 2. The evaporation continues by vapor diffusion from the vaporization plane to the surface (air-dry layer) while it remains hydraulically connected to the drying front below via capillary-induced liquid flow through the so-called film region [4]. With time, the diffusion pathways from the receding vaporization plane become deeper, leading to an insufficient water supply, announcing Stage 3. The drying front during Stage 1 was theoretically analysed. However, a study of its behaviour during Stage 2 and its interaction with the vaporization plane is lacking due to the limitations in the experimental tracing techniques.

Numerous studies focused on the process's influencing factors and addressed the complexity of their interactions. The atmospheric demand at the surface is critical, especially in Stage 1. Nevertheless, the behaviour of the whole process is influenced by the soil properties that define the soil's ability to supply water. The soil properties' impact on the process was investigated in the literature. However, a direct and comprehensive physical soil index, the Pore Size Distribution Index (I_{PSD}), was recently proposed to reflect the soil pore structure and the associated variations in the soil profile properties. Additionally, it was confirmed to be effective in defining the soils' evaporation behaviour [5].

Previous studies have investigated the drying front dynamics during Stage 1, while little is found regarding the vaporization plane and its relation with the drying front. Therefore, the primary objective of this study is to elaborate on the formation and dynamics of the drying front and vaporization plane. Subsequently, investigate the extent of the liquid and vapor pathways within the unsaturated layer during evaporation. A simple yet effective technique involving experimental investigations and image analysis was developed to trace the unsaturated layer. Accordingly, new insights were delineated

* Corresponding author: jumanahusary@gmail.com

regarding the spatial and temporal development of the interfaces and the film region. Finally, the importance of considering a comprehensive pore-scale index to elaborate on the evaporation process is highlighted.

2 Experimental considerations

2.1 Drying column tests

Homogenous sandy soil drying column tests were conducted. A transparent acrylic column of 50 cm height and a rectangular surface area of 49 cm^2 was used for testing. The soil column preparation method, including the dry compaction and saturation steps, was done following the exact steps explained in [5] to ensure a uniform and initially fully saturated soil profile. Different gradations of silica sand were used to vary the soil pore structure. S1 is a K-6 sample, and S2 is a mixture of K-3 and K-5 samples with a 1:1 ratio by weight. A summary of the profiles' properties is shown in Table 1, while their particle size distribution curves are shown in Figure 1a. The Soil Water Characteristic Curves (SWCC) were determined using the Continuous Pressurization Method (CPM) [6-9] and were fitted using the van Genuchten model (VG) [10], as shown in Figure 1b. The pore size distribution curves were inferred from the SWCCs (Figure 1c), and the I_{PSD} was computed as follows [5]:

$$I_{PSD} = \left(\frac{1}{d_1} - \frac{1}{d_2}\right) \times CV \quad (1)$$

$(1/d_1)$-$(1/d_2)$ indicates the PSD width, which considers the capillary flow during Stage 1. d_1 and d_2 are the smallest and largest capillaries, corresponding to the residual and air-entry suction values. CV is the coefficient of variation of the fitted lognormal distribution reflecting the vapor diffusion pathways. Evaporation was allowed from the fully-saturated profile's top surface, as illustrated in Figure 2. Climatic conditions were unified at 28.1±0.5℃ temperature, 44.7±0.6% relative humidity, and 2.3±0.2 m/s wind speed to eliminate the influence of the demand. The column was instrumented with Time Domain Reflectometry probes (TDRs) installed alongside the column's depth and connected to a data logger to record the profile's saturation. All data and boundary conditions were recorded at 120-second intervals during testing.

2.2 Image acquisition and analysis

Several methods were reported in the literature to trace the unsaturated layer during drying, including image analysis, profile saturation, prediction methods, and other numerical solutions [11, 12]. However, those methods are associated with many limitations, such as difficulty taking high-quality images, extracting information related to the dry and saturated layer neglecting the unsaturated layer, using costly tools that are not commonly available in geotechnical laboratories, and other sophisticated techniques that require expertise. Therefore, a new technique was developed to capture high-quality images, and a series of image analysis operations were then used to investigate the unsaturated layer dynamics.

The image acquisition setup included several tools to ensure high-resolution and comprehensible images (Figure 2). The testing column was confirmed to have a

Table 1. Soil profiles' properties.

Soil profile name		S1	S2
Commercial name		K-6	K-3+K-5 (1:1)
Specific gravity	Gs	2.636	2.644
Dry density	ρ_d (g/cm^3)	1.502	1.598
Void ratio	e	0.75	0.65
Effective size	D_{10} (mm)	0.20	0.43
Uniformity coefficient	Cu	1.74	2.35
Pore size distribution index	I_{PSD} (×10^{-4}/μm)	7.88	11.57

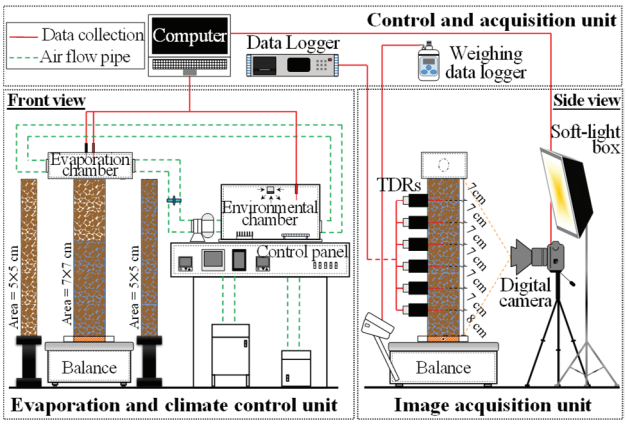

Fig. 2. Experimental setup.

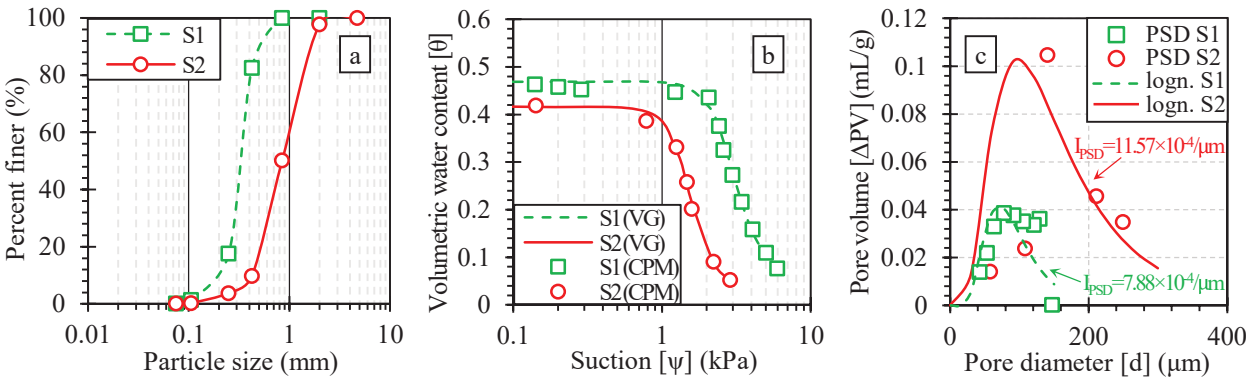

Fig. 1. (a) Particle size distribution curves (b) Soil water characteristics curves (c) Pore size distribution curves.

flat and well-polished surface with minimal scratches to capture the soil profile exclusively and avoid biased results. The profiles were saturated with a commonly used blue dye (brilliant blue, 0.2 g/L) dissolved in water [3]. The blue tracer enhanced the visual contrast between saturated, unsaturated, and dry layers based on blue colour intensity. Fully saturated profiles are dark blue; however, the colour starts fading when water evaporates, and dry soil returns to its original colour with hints of blue dots. Fully saturated and dry reference soil columns were placed next to the primary one, as shown in Figures 2 and 3a. The reference columns were used to calibrate the blue colour intensity for fully saturated and dry soil profiles, allowing the detection of these zones in the primary column. Both were compacted in transparent acrylic columns (50 cm height and rectangular surface area of 25 cm^2) using the same soil gradation and dry density. The saturated column was compacted and saturated as the primary one. The dry column was compacted with dry soil previously saturated with blue water. The reference columns were well sealed from all sides to maintain saturation and colour intensity. 42MP (7952×5304 pixels) high-resolution digital camera connected to a PC was mounted and fixed on a tripod facing the columns to allow remote image acquisition. Finally, two soft light boxes were placed to the sides to unify the light intensity and spread it without causing harsh reflections on the columns' tracing surfaces.

A series of image analysis operations were conducted to detect the drying front and vaporization plane during drying. Firstly, RGB (Red, Green, Blue) acquired images were converted to HSV colour space (Hue, Saturation, Value). The saturation image, which includes the intensity values from 0 to 1, was extracted for further analysis. The average intensities of the saturated and dry soil were determined from the reference columns and were then assigned as threshold values corresponding to the saturated and dry zones in the primary column. Due to the difference in the pore structure and the soil-to-water ratio appearing at the tracing surfaces, the average intensity values varied between S1 and S2. For instance, all values > 0.7 in S2 were considered saturated soil and designated white, while the values < 0.1 were considered dry and designated black. Consequently, the grey colour was considered unsaturated (0.7 < intensity < 0.1). Based on that, two different binary images were generated, all black and all white. The images were carefully improved using morphological opening, an image filtering operation based on the neighbouring pixels' intensities. The resulting images were layered over the original image to make the zones more visible. Finally, a minimum opening operation was conducted on the final image to avoid any essential data loss while refining the boundaries between the zones (Figure 3b).

3 Results and discussion

3.1 Spatial development of the drying front and vaporization plane

The first batch of the analysed images is shown in Figures 4a and 5a for the S1 and S2 profiles, respectively. The information related to the drying front and the vaporization plane was extracted from the images considering the following: 1) the saturated layer is the white connected zone extending from the profile's bottom. 2) The drying front is the interface between the

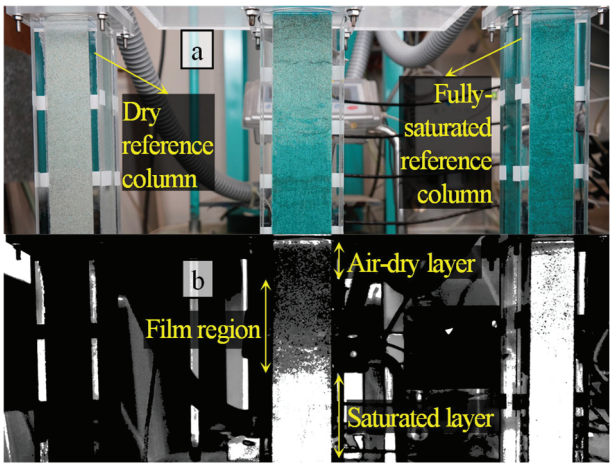

Fig. 3. (a) RGB acquisition image (b) Processed image used for analysis.

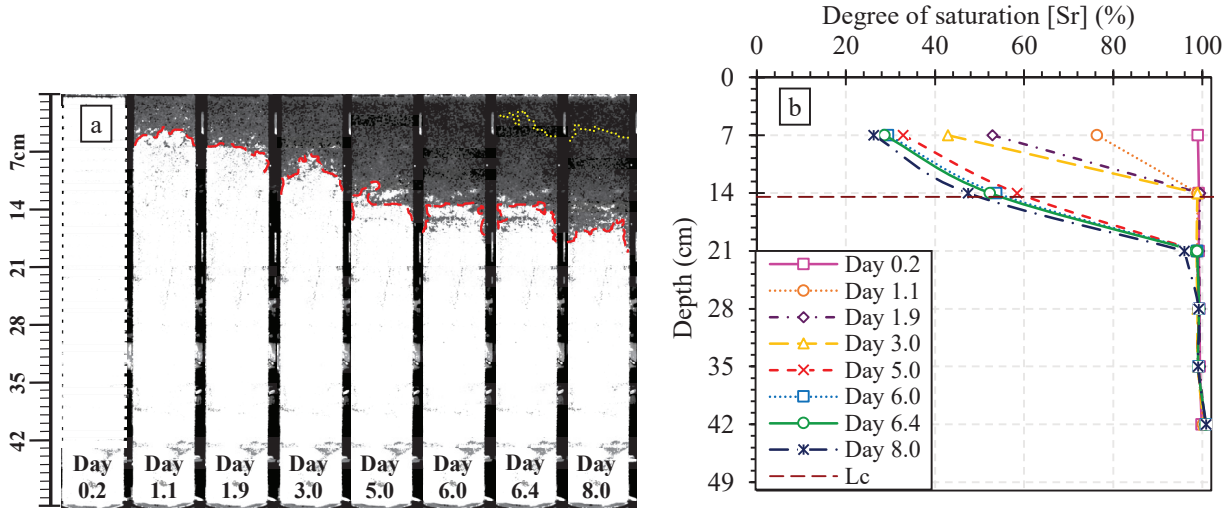

Fig. 4. Early evaporation stages of the S1 profile (a) Processed images (b) Corresponding water redistribution profiles.

white and grey unsaturated zones. The front is delineated with the red line considering all white patches connected to the saturated zone. Consequently, the white patches formed within the grey zone are considered isolated wet clusters, not part of the front. 3) The unsaturated layer or the film region is the connected grey zone involving different shades of grey. Similarly, the isolated black patches within the film region are treated as drying patches, gradually forming drying zones. 4) The air-dry layer is the connected black zone extending from the surface. 5) The vaporization plane is the interface between the grey and black connected zones. The plane is delineated with the yellow dotted line where the disconnected grey patches are not considered part of it. The TDRs' readings were used to plot the water redistribution profiles of S1 and S2, Figures 4b and 5b, respectively. Each line indicates the profile's saturation at which an image was captured. For instance, the white zone corresponds to 100% saturation, and the black zone corresponds to almost residual saturation. These results validate the accuracy and reliability of the new technique.

At the early stages of evaporation, water evaporates from larger pores at the soil surface due to their weaker capillary forces. Once the menisci break, the drying front is formed and starts receding. While the evaporation continues from smaller pores persisting at the surface, water is supplied through capillary liquid flow from the drying front, keeping it connected to the surface. This phenomenon can be observed from the images through the first 6 and 4 days in S1 and S2, respectively. However, the S2 film region included more saturated clusters than S1. However, S1 developed darker shades of grey, reflecting its saturation reduction (Figure 4b). The evaporation continues while pores are drying, and more dry clusters appear within the film region, being more pronounced in S1. The literature mathematically calculated the maximum drying front depth at Stage 1, Characteristic Length (Lc), where the hydraulic connections with the surface are disrupted [3]. For S1 and S2, the Lc equals 14.5 and 6.7 cm, respectively. The drying front was pinned at the Lc between Days 5 and 6 in S1 and Days 2 and 4 in the S2 profile. During these days, dry clusters became more apparent, and the saturation reached near residual values, which led to the hydraulic connections' disruption and the receding of the vaporization plane below the surface, announcing Stage 2.

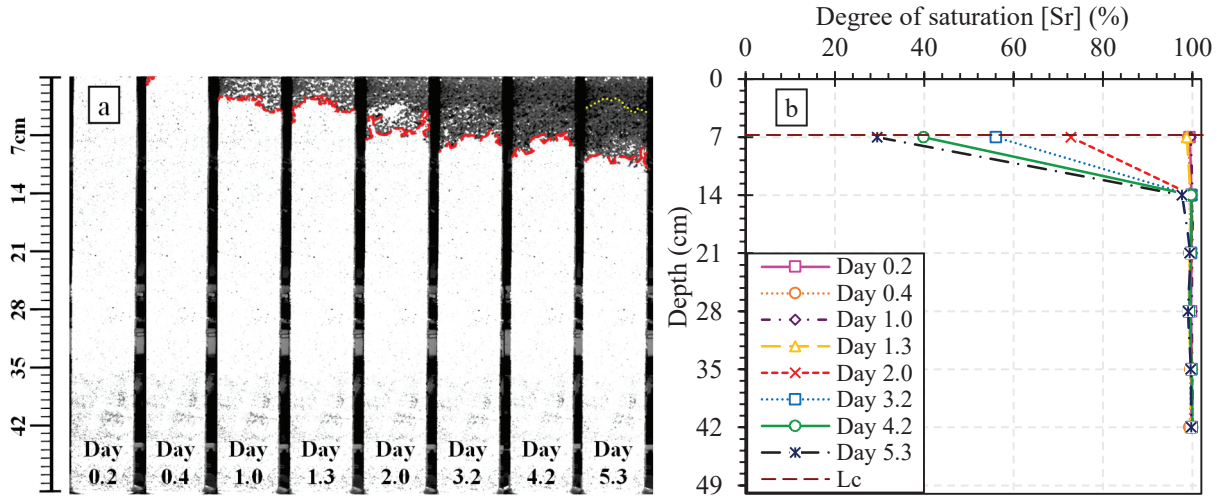

Fig. 5. Early evaporation stages of the S2 profile (a) Processed images (b) Corresponding water redistribution profiles.

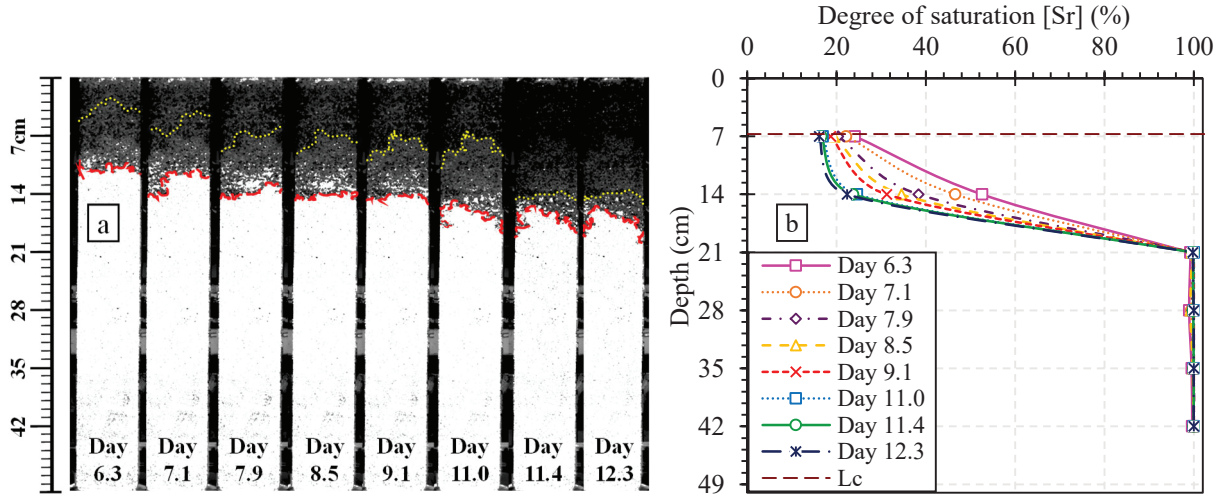

Fig. 6. Late evaporation stages of the S2 profile (a) Processed images (b) Corresponding water redistribution profiles.

Consequently, the unsaturated layer is divided into a film region and an air-dry layer. Water evaporates from the drying front by capillary flow through the film region and then leaves at the vaporization plane by vapor diffusion through the air-dry layer. This behaviour can be seen between Days 6 and 11 in the second batch of images and water redistribution for the S2 profile, shown in Figure 6. The vaporization plane was formed and continued receding along with the drying front. Additionally, the dry layer's grey clusters and the film region's white clusters continuously shrank, and the saturation decreased. Based on that, it can be concluded that during Stage 2, water evaporates mainly from the receding vaporization plane supported by the drying front, which confirms the continued reduction in the evaporation rate due to the increasing distance of the diffusion pathways. Moreover, water also evaporates from the water clusters above the vaporization plane and the film region.

During Day 11, an abrupt increase in the vaporization plane depth was observed, while the drying front showed a slight change. Consequently, an increase in the air-dry layer thickness with almost no grey patches included and a decrease in the film region thickness accompanied this change. This behaviour is believed to be associated with the beginning of Stage 3, where the diffusion pathways from the receding vaporization plane become deeper, leading to an insufficient water supply to the surface.

3.2 Temporal development and geometry of the drying front and vaporization plane

The dynamics and geometry of the drying front and vaporization plane inferred from the images are shown in Figures 7a and 7b, respectively, for both soil profiles. The definition of the notations is explained in the legend of Figure 7a. The top of the interface indicates its shallowest point, while the bottom indicates the interface's deepest point. The determination method of the drying front and vaporization plane's tops and bottoms is explained in the image delineated in Figure 7b. The average between the top and bottom depths defines the interface's average depth, while the difference between the top and bottom depths determines the interface's width.

From Figure 7a, it can be observed that the front behaviour with time was similar for both profiles. The receding rate tends to be faster during Stage 1, with a slight reduction in the rate with each consecutive stage. This behaviour might be attributed to the sufficient water supply during Stage 1, where water is lost directly from the surface, requiring more water to be pumped from the drying front, causing it to recede faster. In contrast, during Stages 2 and 3, the diffusion pathways become deeper, requiring a longer time for a water unit to evaporate. It was observed that S1's drying front receded into deeper layers during Stage 1, while S2's reached the same depth towards the end of Stage 2. Furthermore, the front's top and bottom do not always propagate at the same rate in both profiles, which makes its width variable during drying. However, the irregular fluctuations are more significant in S1, associated with the difference in the pore diameters and its localized distribution. Therefore, it can be concluded that profiles with bigger I_{PSD}, characterized by broader pore distribution, lose water from deeper layers. Moreover, the higher drying fronts' width fluctuations might be associated with the higher possibility of variations in the local pore distribution along the soil profile.

Figure 7b shows that the vaporization plane recedes instantly below the surface at the beginning of Stage 2, followed by a continuous increase in depth with a lower rate towards the consecutive stage. Similarly, an abrupt reduction in depth was noticed at the beginning of Stage 3 in S2. This behaviour explains the sudden drop in the evaporation rate at the onset of Stages 2 and 3, where the diffusion pathways become deeper, requiring more time for water vapor to reach the surface. The vaporization plane dynamics play an essential role during Stages 2 and 3, and its receding rate highly influences the evaporation rate [5]. It was noticed that the vaporization plane recedes to deeper layers in S2 compared to S1, which is the opposite behaviour of the drying front. Therefore, it can

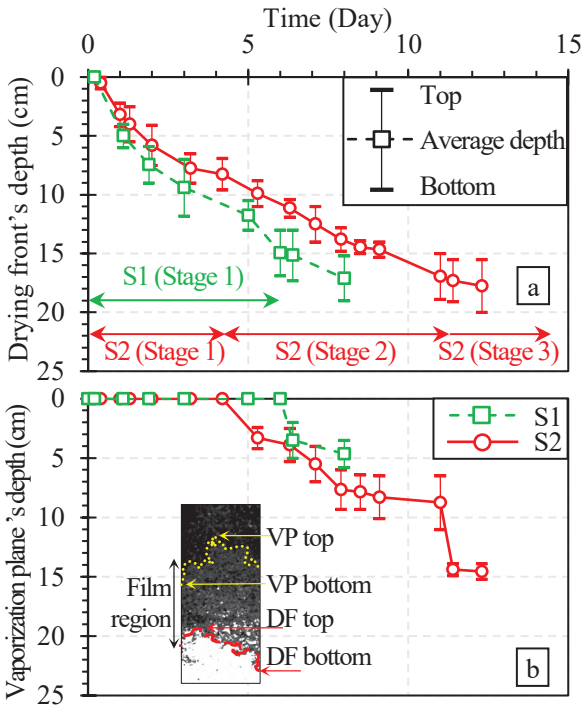

Fig. 7. Temporal development and geometry of (a) Drying front (DF) (b) Vaporization plane (VP).

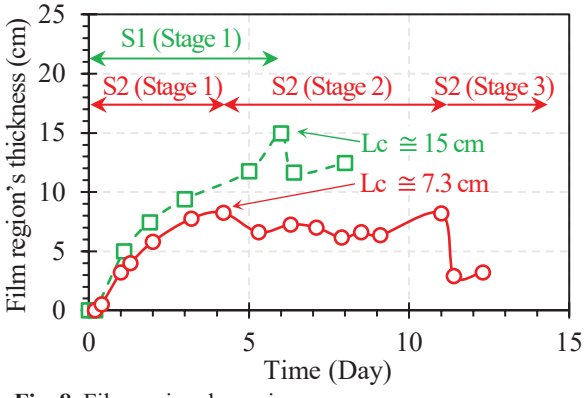

Fig. 8. Film region dynamics.

be concluded that for profiles with bigger I_{PSD}, characterized by broader pore distribution, the vaporization plane is initially formed at shallower depths while continually receding during Stage 2. The plane's top and bottom propagated more constantly than the drying front. However, the plane's width tends to be greater during Stage 2, followed by a distinctly narrower width in Stage 3, which can be seen in the S2 profile.

Since the drying front and the vaporization plane recede during drying, studying the film region is crucial for comprehensively understanding their dynamics. Therefore, the film region thickness was found by taking the difference between the average depths of the vaporization plane and the drying front. The film region thickness for both profiles was plotted with time, as shown in Figure 8. By definition, the film region equals the drying front depth during Stage 1 until the vaporization plane recedes below the surface in Stage 2. For both profiles, the thickness of the film region increased continuously during Stage 1, which equals the drying front depth. However, a slight drop in its thickness can be noticed once reaching the Lc, associated with the onset of Stage 2. During Stage 2, the film region thicknesses slightly fluctuated until reaching a thickness equal to Lc, where a sudden and remarkable second drop in thickness occurred, believed to be the beginning of Stage 3, where the diffusion distance becomes limiting. Consequently, this suggests that each inflection point on the actual evaporation curve might be associated with a significant transition in the film region geometry within the unsaturated soil profile. Therefore, investigating the relationship between the film region dynamics and the pore structure represented by a comprehensive pore index (I_{PSD}) is a fundamental step towards accurately predicting the actual evaporation rates during Stages 2 and 3.

4 Conclusions

Evaporation from soil profiles involves water loss from the soil surface during Stage 1 and from a receding vaporization plane during Stage 2. During both stages, the drying front supplies water through capillary flow, yet during Stage 2, vapor diffusion dominates. The literature studied the drying front during Stage 1. However, a study of its behaviour during Stage 2 and its interaction with the vaporization plane is still lacking. Therefore, this study developed a new technique to elaborate on the formation and dynamics of the drying front and vaporization plane and investigate the extent of the liquid and vapor pathways within the unsaturated soil profiles. The main findings of the study can be outlined as follows:

1. The newly developed technique involves a simple setup to capture comprehensible images and a simple series of image analysis operations to extract information related to the saturated, unsaturated, and dry layers. The technique was proven reliable and accurate, and the resulting images allowed the detection of the drying front, vaporization plane, and film region dynamics.
2. It was found that soil profiles with bigger I_{PSD}, characterized by broader pore distribution, lose water from deeper layers during Stage 1. However, their vaporization plane is formed at shallower depths during Stage 2.
3. The thickness of the film region increased continuously during Stage 1, followed by a slight drop in its thickness once reaching the Lc, associated with the onset of Stage 2. During Stage 2, the thickness slightly fluctuated until reaching a thickness equal to Lc, where a sudden and remarkable second drop in thickness occurred, believed to be the beginning of Stage 3, where the diffusion distance becomes limiting.

This research was partly supported by Grants-in-Aid for Scientific Research (A) 20H00266 and 21K18752 from the Japan Society for the Promotion of Science (JSPS) KAKENHI.

References

1. A. Alowaisy, J. Hussary, N. Yasufuku, R. Ishikura, M. Abdelhadi, J. Arid L. Stud. **32**, S (2022)
2. A. Alowaisy, N. Yasufuku, Lowl. Technol. Int. **20**, 3 (2018)
3. P. Lehmann, S. Assouline, D. Or, Phys. Rev. E **77**, 5 (2008)
4. N. Shokri, P. Lehmann, D. Or, Water Resour. Res. **45**, 10 (2009)
5. J. Hussary, A. Alowaisy, N. Yasufuku, R. Ishikura, M. Abdelhadi, Soils Found. J. **62**, 2 (2022)
6. A. Alowaisy, N. Yasufuku, R. Ishikura, M. Hatakeyama, S. Kyono, *Rapid determination of the unsaturated hydraulic conductivity for sandy soils utilizing the continuous pressurization method*, in Proceedings of The 20th International Conference on Soil Mechanics and Geotechnical Engineering, ICSMGE, 1-5 May 2022, Sydney, Australia (2022)
7. A. Alowaisy, N. Yasufuku, R. Ishikura, M. Hatakeyama, S. Kyono, Soils Found. J. **60**, 3 (2020)
8. A. Alowaisy, N. Yasufuku, R. Ishikura, M. Hatakeyama, S. Kyono, *Novel rapid measurement system of undisturbed soils water characteristics curve utilizing the continuous pressurization method*, in Proceedings of The 7th International Symposium on Deformation Characteristics of Geomaterials, 26-28 June 2019, Glasgow, UK (2019)
9. A. Alowaisy, N. Yasufuku, R. Ishikura, M. Hatakeyama, S. Kyono, *Rapid concurrent measurement of the soil water characteristics curve and the hydraulic conductivity function utilizing the continuous pressurization method*, in Proceedings of The 7th Asia-Pacific Conference on Unsaturated Soils, 23-25 August 2019, Nagoya, Japan (2019)
10. M. T. Van Genuchten, Soil Sci. Soc. Am. J., **44**, 5 (1980)
11. J. Hussary, A. Alowaisy, N. Yasufuku, R. Ishikura, M. Abdelhadi, J. Arid L. Stud. **32**, S (2022)
12. N. Shokri, P. Lehmann, P. Vontobel, D. Or, Water Resour. Res. **44**, 6 (2008)